Tailoring collaborative N-O functionalities of graphene oxide for enhanced selective oxidation of benzyl alcohol

Jiaquan Li,[†] Fuqing Li, [†] Qi Yang,[†] Shaobin Wang,[†]* Hongqi Sun,[‡] Qingning Yang,[§] Junwang Tang,[§]* and Shaomin Liu[†]*

[†] WA School of Mines: Minerals, Energy and Chemical Engineering, Curtin University, WA 6102, Australia.

[‡] School of Engineering, Edith Cowan University, Joondalup, WA 6027, Australia.

[§] Department of Chemical Engineering, University College London, Torrington Place, London, WC1E7JE, UK

[#] Department of Chemical Engineering, Monash University, Clayton, VIC 3800, Australia

ABSTRACT. Benzaldehyde (BzH) is one of the most important chemicals in industrial feedstock. However, the conventional production processes heavily rely on precious metal catalysts and bring about unavoidable pollution issues. Here we report a new catalytic process to use N-doped graphene oxide as the catalyst to oxidize benzyl alcohol (BzOH) into BzH by an environmentally benign oxidant, peroxymonosulfate (PMS) under mild conditions . The optimized catalyst could achieve 96% BzOH conversion and unprecedented 82% BzH yield under benign conditions, superior to the precious metal (Pd) catalsyts reported. Such attractive performance is believed due to the electron-withdrawing pyridinic N and electron-donating C=O on the catalyst which either forms an electron bridge for the electron transfer between BzOH and the oxidant via a non-radical pathway or separately induce the generation of free radicals from PMS to accomplish the radical pathway. Furthermore the yielded BzH was free from over-oxidation under various reaction conditions in both radical and non-radical perspectives despite its inherently high activity, thus favoring the high selectivity. This work

25 provided a mechanic understanding of carbocatalysis for green organic synthesis with

26 environmental and economic perspectives.

27 **KEY WORDS**: N-doped graphene; benzaldehyde; selective oxidation; dual active sites; electron

28 transfer.

29

30 **INTRODUCTION**

31   Selective oxidation of benzyl alcohol (BzOH) to benzaldehyde (BzH) is an important route to

32 manufacture high value-added organic products.[1] Excellent efficiency has been achieved using

33 conventional catalysts such as noble metals in O_2. However, there are two drawbacks of these

34 conventional methods. One is that noble metals are too expensive for real applications,[2-3] and the other

35 one is that due to the inertness of O_2 molecules, high reaction temperature or addition of promoters

36 such as HNO_3 is required to attain an ideal BzH yield. In order to tackle those problems, low-cost

37 transition metals and nanocarbons could be applied as alternative catalysts.[4-9] Also, peroxide oxidants

38 such as hydrogen peroxide (H_2O_2), *tert*-butyl hydroperoxide (TBHP), and peroxymonosulfate (PMS,

39 basically available as a triple salt of potassium $KHSO_5 \cdot 1/2KHSO_4 \cdot 1/2K_2SO_4$, oxone) have been

40 studied for liquid-phase organic oxidation reactions to replace oxygen gas.[10-12] These peroxides can

41 be activated under mild conditions for oxidative reactions. However, liquid H_2O_2 and TBHP may have

42 safety issues and high cost in transportation and storage, and because of that, PMS as a chemically

43 stable crystal solid has received intensive attention for both selective and non-selective oxidation

44 reactions.[13] PMS has an excellent potential for numerous fundamental reactions of synthetic chemistry

45 such as the selective oxidation of C-H bonds of olefins and alcohols to obtain the corresponding

46 oxygenated compounds.[10] However, extra additives are required to activate PMS to form more

47 reactive and selective oxidizing species to accomplish a high yield of target products in these cases.[14-

48 20]

49   In recent years, activation of PMS by carbon-based metal-free catalysts have been proposed and

50   extensively studied in the advanced oxidation processes (AOPs) for water treatment.[21] The sp^2

51   hybridized carbocatalysts with surface carbonyl groups can induce the generation of various radicals

52   including $SO_4^{\bullet-}$ (2.5-3.1 V), $SO_5^{\bullet-}$ (1.1 V) and $^\bullet OH$ (2.7 V), which can non-selectively attack the

53   aqueous organics.[22-25] Furthermore, non-radical AOPs owing to the direct electron transfer from the

54   target organics to PMS via the sp^2 carbon framework has also been reported.[26] However, most of these

55   studies of PMS activation by carbocatalysts are reported for wastewater treatment but rarely applied

56   for organic synthesis. Unlike the radical-based AOPs, the non-radical pathway sheds lights on the

57   feasibility of applying PMS in the selective oxidation. Via catalyst modification, the electron transfer

58   ability and oxidative potentials of the PMS-carbocatalyst-organic substrate system can be tailored to

59   replace the precious metal catalysts and expensive/unstable oxidants, thus achieving the selective

60   oxidations in an environmentally-benign manner.

61   Previously, we reported carbon nanotubes for PMS activation for the selective oxidation of BzOH.[27]

62   Dominated by a radical process, this facile reaction could be conducted under benign conditions

63   without adding any other co-catalysts or additives. However, the BzH yield was still not ideal due to

64   deep oxidation of BzOH by radicals reducing the selectivity to BzH. Thus, it was inspiring to improve

65   oxidative efficiency via non-radical routes. BzH was known to be unstable owing to the presence of

66   the aldehyde group and readily suffers from autoxidation into benzoic acid (BzOOH) even under air

67   exposure.[28] Therefore, over-oxidation was a major concern with the presence of BzH for the selective

68   oxidation of BzOH. Very unexpectedly, no by-product of BzOOH was detected, mirroring that further

69   oxidation of the formed BzH was unlikely to occur in the carbon nanotube/PMS system.[27] Therefore,

70   the reaction behaviour of BzOH and BzH towards the radical/non-radical oxidation by PMS deserved

71   further research to gain a comprehensive understanding of the intrinsic reaction mechanism and to

72   provide guidance for the catalyst design.

73   Nitrogen-doped carbon materials have been reported as efficient metal-free catalysts for PMS

74   activation in AOPs, especially via the non-radical pathway.[26] The nature of carbon catalysts, including

75   the surface functional groups and the electrochemical properties, could be tailored for improved

76   catalytic efficiency. However, the identification of active sites on doped graphene catalysts was

77   usually focused on either N or O species. At the same time, the integrated study regarding the

78   synergistic effect of different functional groups on the catalytic performance has rarely been reported.

79   Herein, we report the application of N-doped graphene oxides (NGO)/PMS for highly selective

80   oxidation of BzOH towards BzH with over 95% selectivity. The non-radical oxidation process was

81   enhanced by tuning the surface functionalities to gain a high BzH selectivity. The different reaction

82   pathways towards the oxidative NGO/PMS system were explored deeply via comprehensive

83   experimental and computational work. The protective role of BzOH against the undesired over-

84   oxidations was also clarified. Thus, the current work paved a new way for highly efficient and green

85   carbocatalysis for organic synthesis.

86   **MATERIALS AND METHODS**

87   **Materials.**

88   Graphite powder, active carbon (AC) and nanodiamond (ND) were purchased from Sigma Aldrich.

89   Multi-walled carbon nanotubes (MWCNTs) and single-walled carbon nanotubes (SWCNTs) were

90   purchased from Timesnano, Chengdu, China. The peroxide hydroxide (~30 %) was obtained from

91   Chem-supply. The other chemicals were supplied by Sigma Aldrich.

92   **The preparation of N-doped carbocatalysts.**

93   Graphene oxide (GO) was prepared by the Hummers' method from graphite. The synthesis of N-

94   doped graphene (NGO) was carried out by impregnation and annealing. In a typical process, 1 g GO

95   was finely ground and mixed with 1 g urea in a certain amount of water. The mixture was maintained

96   at room temperature for 12 h and then dried at 60 ℃. The product was annealed at 400 ℃ for 2 h

97   under N_2 protection in an electric furnace. Then the black powder was fully washed by water and

98   ethanol and dried at 60 ℃ for 24 h to obtain NGO.

99   Other carbon substrates were prepared by the following procedures. One gram MWCNTs (or

100   SWCNTs/ND) were added into a mixture of 15 mL HNO_3 (65-68%) and 45 mL H_2SO_4 (95-98%) and

101   sonicated at 25 ℃ for 5 hours. Then the precipitate was filtered and thoroughly washed with deionized

102   water. The black carbon nanotubes were dried at 60 ℃ for 48 h to obtain O-MWCNT (O-SWCNT or

103   O-ND). Then the O-MWCNT, O-SWCNT, AC and O-ND were employed as different carbon sources

104   to prepare the corresponding N-doped carbocatalysts with a similar process as NGO. In addition,

105   N(Melamine)-GO and N(NH_4NO_3)-GO were also synthesized by replacing urea with the same mass

106   loading of melamine and NH_4NO_3 as N precursors.

107   Hydrogen peroxide, PMS and $KMnO_4$, were then used as oxidants for the post-oxidation treatments

108   of NGO, separately. For the synthesis of NGO-H_2O_2, 0.5 g NGO was added into 50 mL H_2O_2 and

109   stirred under 50 ℃ for 5 h. After cooling down, the precipitate was filtered, washed with deionized

110   water and dried at 60 ℃ for 24 h. The formation of NGO-PMS and NGO-$KMnO_4$ were carried out

111   with a similar method and the mixture was composed of 0.5 g NGO, 0.5 mol oxidant and 50 mL water.

112   The preparation of C=O-rich NGO with inorganic additives (NGO-A/N, NGO-A/Cl, NGO-A/C,

113   NGO-Mg/N, NGO-Fe/N and NGO-Ca/N) was conducted with the same procedure as NGO except

114   that 3.8 mmol of inorganic salts were added into the mixture at the impregnation step.

115   **The passivation of carbonyl groups.**

116   The elimination of carbonyl groups on NGO and NGO-H_2O_2 was conducted in the following

117   process. Firstly, 0.5 g phenylhydrazine (PH) and 100 μL HCl (38%) were dissolved in 10 mL $CHCl_3$,

118   followed by adding 0.1 g NGO. The mixture was stirred under N_2 atmosphere at 60 ℃ for 48 h in

119   dark. The precipitate was then thoroughly rinsed with $CHCl_3$ and ethanol to remove the residual PH.

120   Then the solid was dried at 60 ℃ for 24 h to obtain NGO-PH. The NGO-H_2O_2-PH was prepared in a

121   similar procedure.

122   **Selective oxidation of BzOH.**

123   The catalytic evaluations of selective oxidation of BzOH were performed as follows. In a typical

124   catalytic process, 5 mg catalyst was mixed with 2.5 mL acetonitrile and 2.5 mL water in a flask and

125   maintained under sonication for 5 min. Then 0.1 mmol BzOH and 0.11 mmol oxone were added into

126   the mixture. The flask was sealed and maintained at 50 ℃. After 5 h, the reactor was cooled down

127   followed by the injection of 0.1 mmol anisole as an internal standard. The mixture after the reaction

128   was filtered and the organic phase was extracted by toluene and analyzed with GC.

129   **Theoretical calculations.**

130   The simulation of adsorption of molecules on graphene templates was carried out by spin-

131   unrestricted density functional theory (DFT) calculations. A Dmol3 package was employed using

132   general gradient approximation (GGA) with Perdew-Burke-Ernzerhof (PBE) as the exchange-

133   correlation function. Double numerical plus polarization (DNP) was applied as the basis set and the

134   DFT-D method within the Grimme scheme was selected to take account of the van der Waals forces.

135   When simulating the adsorption behaviour of BzOH and PMS molecules on different graphene

136   models, the adsorption energies were calculated from the following equations, respectively.

137    $E_{ads}(BzOH)=E_{BzOH/G}-(E_{BzOH}+E_G)$

138   and

139     $E_{ads}(PMS)=E_{PMS/G}-(E_{PMS}+E_G)$

140   Where the $E_{BzOH/G}$, $E_{PMS/G}$, E_{BzOH}, E_{PMS} and E_G are the energies of the BzOH/graphene system,

141   PMS/graphene system, isolated BzOH molecule, PMS molecule and graphene, respectively.

142   **Characterizations.**

143   Transmission electron microscopy (TEM) images were obtained by a JEOL 2100 microscope.

144   Scanning electron microscope (SEM) images were conducted on a Zeiss Neon 40EsV FIBSEM.

145   Raman spectra of graphene samples were obtained under ambient conditions on a Renishaw Raman

146   spectrometer with a 785 nm laser beam. X-ray photoelectron spectroscopy (XPS) analysis was

147   performed on a Kratos AXIS Ultra DLD system with Al Kα radiation and a base pressure of 1×10^{-8}

148   torr. The binding energies were referenced to the C1s line at 284.6 eV from defect-free graphite.

149   **RESULTS AND DISCUSSION**

150   In order to fundamentally understand the significant roles of the individual functional groups (i.e.,

151   N and O species) on the catalysts in the catalytic reactions, a series of techniques were employed to

152   modify graphene with varying functionalities and contents. In addition to the major reactions from

153   BzOH to BzH using the NGO/PMS system, other oxidations such as employing BzH as the reactant

154   with or without the competing substrates were also performed in combination with density functional

155   theory (DFT) calculations to fully understand the oxidation behaviour.

156   **Design and synthesis of carbocatalysts with tailored N-O functionalities.**

157   Urea was chosen in this work as it was one of the superior N precursors for the preparation of N-

158   doped carbocatalysts in PMS activation.[29] The selective oxidation reaction of BzOH was performed

159   in acetonitrile/water solution at a moderate temperature (50 ℃) in the presence of PMS. Several

160 carbon substrates were employed including GO, MWCNTs, SWCNTs, AC and ND. The

161 corresponding N-doped catalysts were synthesized by an incipient impregnation and thermal

162 decomposition method. The effects of the N doping into different carbon materials on the catalytic

163 performance were investigated (Table S1). N doped GO achieved 22-fold enhancement of BzH yield

164 (33.6%) compared with N-free GO (1.5%), while for the other carbon materials, the enhancement was

165 below 3-fold. The information of N content on the catalysts was obtained from an elemental analysis

166 of the XPS survey. With equal urea loading amount (1.0 urea:1.0 carbon source, mass ratio), the

167 surface N content in N-doped GO reached 9.6% while for the other carbons, the N content was less

168 than 3.1%, indicating that the morphological or structural nature of GO was superior to the other

169 carbons in accommodating more surface N species. The influence of the N precursor loading (urea,

170 from 10 to 200 wt.%) suggested that, at the weight ratio of urea/GO over 1, the content of N species

171 on N-doped GO was saturated and the catalytic performance showed no obvious change with the

172 further increased urea dosage (Figure S1). In this sense, the N-doped GO prepared with an equal mass

173 ratio of urea:GO (denoted as NGO) was selected as the catalyst for subsequent investigation and

174 discussion.

175 After urea doping, the oxygen level of GO substantially dropped from 28.8 to 8.2%. In comparison,

176 a control sample (GO-400) was prepared with the same procedure as NGO but without urea loading.

177 The oxygen concentration of GO-400 (15.0%) exceeded NGO (8.2%) by a large scale, indicating that

178 the oxygen groups were replaced by N species during the N doping. Notably, both BzOH conversion

179 and BzH selectivity increased with higher N dosage, indicating the incorporated N species might result

180 in higher conversion/selectivity. SEM and TEM images (Figure S2a, b) revealed the morphology of

181 highly exfoliated graphene sheets with winkled structures, which were commonly observed on N-

182 doped graphene.[23, 29] The nano-scaled thin layer structure enabled fast mass and charge transfer during

183 the catalytic reactions. Further high-angle annular dark-field scanning (HAADF-STEM) images

184   (Figure S2c left) and elemental mapping (Figure S2c, right) indicated that the abundant N and O

185   species were uniformly distributed on NGO.
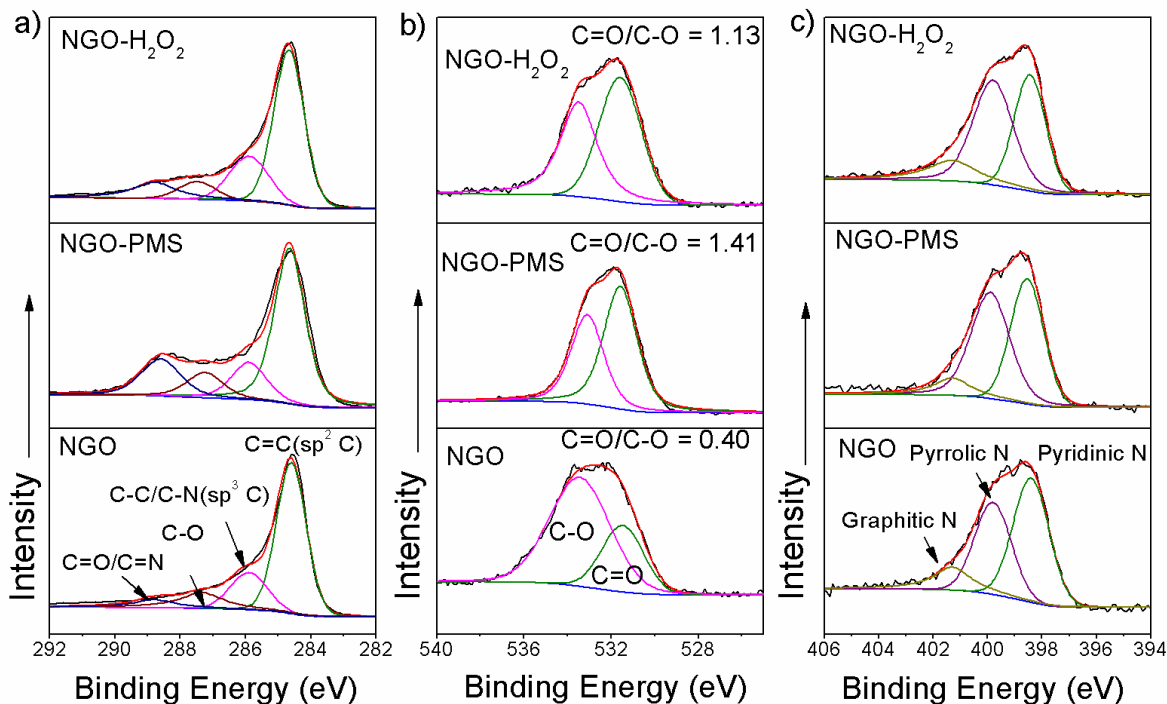
186
187   **Figure 1.** Deconvolution of a) C 1s, b) O 1s and c) N 1s XPS spectra of NGO, NGO-PMS and

188   NGO-H₂O₂.

189   The N species on N-doped carbon materials were dominantly classified into three kinds of species,

190   namely graphitic or quaternary N, pyrrolic N and pyridinic N.[30-32] Previous research suggested that

191   the quaternary N served as the active site for PMS activation in AOPs, especially endowing the non-

192   radical pathway.[26] Besides, the electron-rich C=O groups were regarded as an electron donor to

193   activate PMS. However, there was still a lack of a comprehensive understanding of the catalytic role

194   of different N species and the correlation between the surface N and O groups. It was recently found

195   that the electron affinity (electrophilic and nucleophilic) of surface functionalities on the catalyst

196   played a significant role in PMS activation for selective oxidation of BzOH by facilitating the electron

197   transfer between the PMS and carbon catalysts.[27] In this regard, it was a logical consideration to

198   develop highly-active carbon catalysts with an electron bridge of dual electron mobility to further

199   promote the electron transfer from the target organics to PMS.

200   The surface chemistry of NGO was investigated by XPS (Figure 1). The deconvolution of N 1s

201   spectra of NGO presented the pyridinic N at 50% of the whole N content, whereas the quaternary N

202   only contributed 14% (Figure 1c, bottom). It has been reported that the pyridinic N could induce p-

203   type domains on graphene oxide to withdraw electrons from the adsorbed electron-rich molecules.[33]

204   In this sense, the electron-withdrawing pyridinic N and electron-donating C=O groups might facilitate

205   adsorption of BzOH/PMS to form an electron tunnel for the electron transfer from BzOH to PMS

206   through the graphene framework. The O 1s XPS spectra could be fitted into two peaks of C-O and

207   C=O species with a relatively low C=O/C-O ratio of 0.4 (Figure 1b, bottom), indicating that the

208   surface oxygen functionalities on NGO were dominantly composed of C-O species. The C-O/C=O

209   ratio of carbon materials significantly relied on the oxidizing environment,[34-35] which enabled the

210   improvement of catalytic performance via optimizing the N and O functionalities.

211   In order to increase the concentration of C=O groups on NGO, a hydrothermal-oxidation treatment

212   was firstly carried out using three typical oxidants (H_2O_2, $KMnO_4$ and PMS) and the samples were

213   denoted as NGO-H_2O_2, NGO-$KMnO_4$ and NGO-PMS, respectively. The N content of the catalysts

214   and their catalytic activities in the selective oxidation of BzOH were summarized in Table 1. GO was

215   ineffective in BzOH oxidation (entry 2) compared with the catalyst-free test (entry 1). Annealed GO

216   without urea dopant (GO-400, entry 3) barely improved the catalytic performance. N doping on GO

217   (NGO, entry 4) profoundly increased the BzOH conversion (42.9%) and BzH yield (33.6%) with a

218   relatively high selectivity of 78.3%, indicating that the enhanced catalytic activity of NGO was

219   attributed to the N doping, and the oxygen functional groups alone could scarcely activate PMS. The

220   post-oxidation of NGO further increased catalytic performances. Notably, the BzH selectivity kept

221   over 90% for the three samples (entries 6,7,8). Among these three catalysts, NGO-$KMnO_4$ presented

222   the lowest improvement in both BzOH conversion and BzH yield because $KMnO_4$ caused a severe

223 loss of the surface N species (from 9.6 to 2.4%, XPS). The BzH yield of NGO-H_2O_2 reached 52.2%.

224 However, GO-400-H_2O_2 presented no improvement in catalytic activity (entry 5), reflecting the

225 indispensable role of N doping in the post-oxidation treatment. The further oxidation of BzH into

226 BzOOH was excluded as BzH was the only organic product detected from GC-MS analysis.

227 **Table 1.** N and O content and catalytic performance of different catalysts in selective oxidation of

228 BzOH[a]

Entry	Catalyst	N/O content (at.%)[b]	BzOH conversion (%)	BzH selectivity (%)	BzH yield (%)
1	-	-	10.2	8.8	0.9
2	GO	-/28.8	9.7	8.2	0.8
3	GO-400	-/15.0	8.2	18.3	1.5
4	NGO	9.6/8.2	42.9	78.3	33.6
5	GO-400-H_2O_2	-/18.4	8.6	25.1	2.2
6	NGO-PMS	9.2/20.1	48.7	91.3	44.5
7	NGO-$KMnO_4$	2.4/27.5	45.8	93.2	42.7
8	NGO-H_2O_2	10.5/9.4	56.1	93.1	52.2
9	NGO-PH	10.8/8.0	31.2	60.5	18.9
10	NGO-H_2O_2-PH	13.6/7.7	30.7	55.7	17.1
11[c]	NGO-A/N	7.5/10.3	62.0	95.3	59.1
12[d]	NGO-A/N	7.5/10.3	96.0	85.4	82.0

229 [a] Reaction conditions: 5 mg catalyst, 0.1 mmol BzOH, 0.11 mmol PMS, 5 mL acetonitrile 1:1 water
230 (volume ratio), 50 ºC, 5 h.
231 [b] Surface N and O concentrations on fresh catalysts derived from XPS.
232 [c] The reaction time was 3 h.
233 [d] The reaction time was 3 h and the PMS loading was 0.25 mmol.

234
235 Raman spectra were adopted to evaluate the graphitic degree of the graphene-based catalysts with

236 the ratio of D and G peak intensities I_D/I_G as an indicator (Figure S3).[36] After the N-doping, the I_D/I_G

237 increases from 1.09 (GO) to 1.42, but the post-oxidation with H_2O_2 caused a negligible increase of

238 I_D/I_G (1.44). It could be inferred that the enhanced catalysis after the post-oxidation treatment was not

239 induced by the variation of structural defects. The total oxygen content of NGO increased after post-

240 oxidation treatments (Table 1), mirroring the occurrence of re-oxygenation of the NGO. The

241 deconvolution of C 1s,[37-38] O 1s [34] and N 1s [6] XPS spectra were applied to reveal the revolution of the

242 surface N and O states before and after the post-oxidation treatment. For the C 1s (Figure 1a) XPS

243 spectra of NGO, NGO-PMS and NGO-H_2O_2, the latter two samples had stronger C=O/C=N peaks.

244 The O 1s XPS spectra (Figure 1b) further confirmed that the post-oxidation treatment led to the

245 conversion of C-O into C=O on NGO with a higher C=O/C-O ratio (NGO: 0.40, NGO-PMS: 1.41 and

246 NGO-H_2O_2: 1.13) whereas there was no visible variation of the composition of N species (Figure 1c).

247 From the above results, the C=O groups were suggested playing a critical role in N-doped graphene

248 catalysis and synergistically work with the active N species for PMS activation.

249 **Identification of active sites and mechanism of the catalytic routes.**

250 For identifying the catalytic roles of active N and O species and reaction pathway, different N

251 precursors (melamine and NH_4NO_3) were used to prepare more NGO and H_2O_2 treated NGO samples.

252 The XPS elemental analysis, N 1s deconvolution species and the catalytic performance of the relevant

253 catalysts, were presented in Table S2 and Figure S4. The N content on melamine derived N-GO was

254 as high as 36.2%, dominantly composed of graphitic N (71%) together with 17% pyrrolic N and 12%

255 pyridinic N. The BzH yield on melamine derived N-GO reached 29.6%, slightly lower than that by

256 urea derived NGO (33.6% BzH yield with 9.6% N content). However, after post-oxidation by H_2O_2,

257 the N content slightly reduced to 33.7% without apparent changes in the composition of each N species,

258 and the BzH yield decreased to 24.5%. For NH_4NO_3 derived N-GO, the total N concentration was

259 6.4% and was composed of pyrrolic (38%), pyridinic (39%) and graphitic (23%) N. After H_2O_2

260 treatment, a considerable loss of pyridinic N occurred (graphitic N: 32%; pyrrolic N: 42%; pyridinic

261 N: 26%; total N content: 4.2%), probably due to the unstable N-graphene configuration derived from

262   NH_4NO_3. As a consequence, the BzH yield dramatically decreased from 16.7 to 4.2%. These results

263   further confirmed the pivotal role of pyridinic N on N-GO in PMS activation for BzOH oxidation.

264   The carbonyl groups on carbon materials could be selectively deactivated by phenylhydrazine (PH)

265   via a particular reaction (Figure S5).[39] The C=O groups reacted with hydrazine to form a -C=N-N-

266   structure, thus leading to the increased N concentration. Both NGO and NGO-H_2O_2 underwent C=O

267   deactivation, and the N/O contents before and after the C=O deactivation were illustrated in Table 1,

268   entries 9 and 10. For NGO-H_2O_2, the increase of N concentration (3.1%) and decrease of O

269   concentration (1.7%) after the PH treatment was more significant than these of NGO (1.2% and 0.2%),

270   confirming that the C=O species on NGO were enriched after H_2O_2 post-oxidation. As expected, NGO

271   and NGO-H_2O_2 suffered from a sharp decrease in both BzOH conversion and BzH selectivity owing

272   to the deactivated C=O groups. Notably, the PH treated NGO and NGO-H_2O_2 shared similar levels of

273   catalytic efficiency, revealing that the enhanced catalytic performance by post-oxidation was

274   attributed to the additional C=O groups to incorporate with C=N. At this stage, the essential role of

275   C=O species on NGO was verified and C=O was responsible for the improved conversion/selectivity.
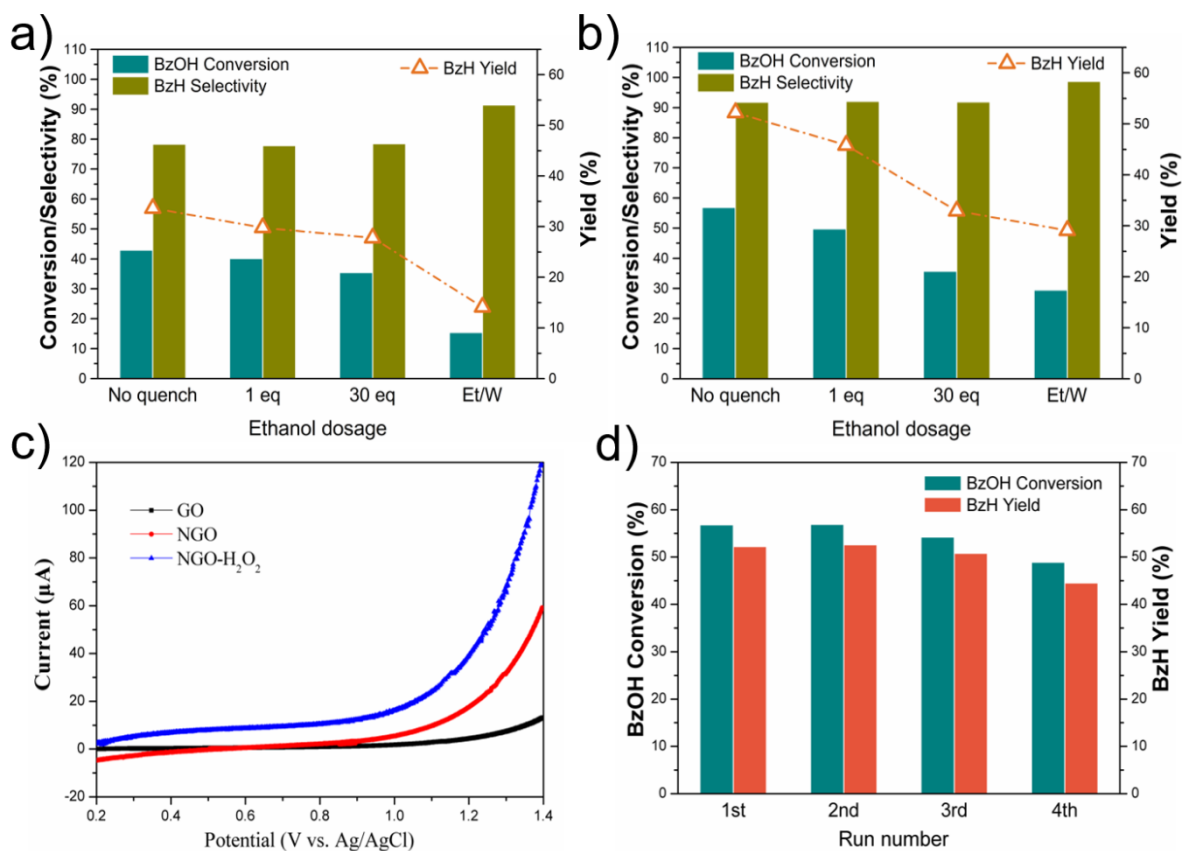
Figure 2. The influences of ethanol dosage on the selective oxidation of benzyl alcohol with a) NGO and b) NGO-H_2O_2. The ethanol dosages were set as 1 equivalent of PMS (1eq), 100-fold of PMS (100 eq) and replacing the acetonitrile solvent with ethanol (Et/W), respectively. c) Linear-sweep voltammograms of different catalysts. d) Stability and recycling test of NGO-H_2O_2. Reaction conditions of a), b) and d): 5 mg catalyst, 0.1 mmol BzOH, 0.11 mmol PMS, 5 mL acetonitrile/water (1:1, volume ratio), 50 ℃, 5 h.

A series of quenching tests were also performed for an in-depth understanding of the reaction pathways (radical/non-radical) in this system. Ethanol was employed as a strong quenching agent for both hydroxyl and sulfate radicals while *tert*-butanol (TBA) served as an effective ˙OH scavenger.[27] The quenching effect of ethanol dosage on NGO and NGO-H_2O_2 was presented in Figure 2a and 2b. A rapid drop of BzOH conversion and BzH yield was observed with increased dosage of ethanol, indicating that the radical process was still vital in selective oxidation of BzOH. When the acetonitrile in the solvent was completely replaced by ethanol, the BzH selectivity increased remarkably and NGO-H_2O_2 possessed a higher BzH yield (29.1%) than NGO (14.1%). A similar trend with a much

14

292 slower deteriorating speed of the catalytic performance was found when we replaced ethanol with

293 TBA (Figure S6). Therefore, sulfate radicals were suggested to be mainly responsible for the selective

294 oxidation of BzOH through the radical pathway, while hydroxyl radicals made a minor contribution.

295 Moreover, the different contributions of radical and non-radical processes to the BzH yield could also

296 be roughly determined by assuming that the BzH yield in the maximum ethanol dosage experiment

297 was completely due to the non-radical reaction. It turned out that both the radical and non-radical

298 processes were enhanced after post-oxidation of NGO and the non-radical reaction rate showed a more

299 significant increment than radical reaction (Figure S7). It could be inferred that the radical and non-

300 radical processes were simultaneously facilitated via the enrichment of C=O groups and the non-

301 radical oxidation contributed more in selectively transforming BzOH into BzH than the radical

302 process. Likewise, the role of N species in affecting the radical/non-radical process was investigated

303 by altering the N (urea) dosage during NGO preparation (from 10 to 100%, Figure S8). Similarly,

304 both radical and non-radical reaction rates increased at a higher N content. This revealed that the C=O

305 and N species were actively involved in both radical and non-radical oxidation reactions. The

306 mechanism will be explored and discussed shortly.

307   As the carbocatalyst-mediated electron transfer was crucial for the non-radical pathway, linear

308 sweep voltammetry (LSV) tests were conducted to check the electrochemical properties of the

309 catalysts. As shown in Figure 2c, in the presence of PMS/BzOH, the electron transferability of the

310 catalysts followed an order of NGO-H_2O_2 > NGO > GO, agreeing well with the catalytic performance

311 especially in the level of non-radical oxidation. Since the C=O groups alone were unable to activate

312 PMS (as previously discussed), it was supposed that either the radical or non-radical pathway relied

313 on the electron transfer between C=O and pyridinic N. In addition, NGO-H_2O_2 possessed better

314 stability in comparison with our previously reported carbocatalysts[27] as it showed no significant

315 reduction of catalytic activity after 4 runs (Figure 2d). In other words, the N and O dual active sites

were well maintained during the reaction without electron accumulation, implying that the carbocatalysts could act as an electron bridge.

Preparation of the C=O-rich NGO with inorganic additives.

For further confirmation of the hypothesis, a one-step method was developed to prepare C=O-rich NGO catalyst from GO to introduce N dopant and prosper the C=O groups simultaneously with extra additives during the preparation. A solid-state synthesis method has been reported, employing magnesium nitrate to produce reduced GO and annealed CNTs based MgO-nanocarbon hybrids with a high C=O concentration.[40-41] In this work, both non-metallic salts including NH_4NO_3 (A/N), NH_4Cl (A/Cl), NH_4HCO_3 (A/C) and metallic salts were applied individually as additives with urea to prepare NGO. The ketonic C=O content was greatly enhanced and encroached on the proportion of C-O/O=C-O groups by the addition of non-metal salts (Figure S9a). Likewise, similar results were observed when replacing the non-metal salts with $Mg(NO_3)_2$, $Ca(NO_3)_2$ and $Fe(NO_3)_3$ (Figure S10). It was inferred that loading either non-metallic or metallic salts into the NGO preparation could enrich the ketonic C=O groups, possibly due to the etching of graphene sheet by the decomposition of the salt, which led to more defect sites for the selective generation of C=O. In contrast, the nitrogen showed no significant compositional variation by the additives (Figure S9b). In terms of the catalyst evaluation, different inorganic salts presented a unanimous contribution to enhancing the catalytic efficiency (Table 1, Table S3). The BzH yield was raised to above 50% with over 90% selectivity for all the catalysts. NGO-A/N showed the best reactivity after 3 h reaction at the PMS/BzOH molar ratio of 1.1 to generate BzH in 59.1% yield and 95.3% selectivity, which was superior to NGO-H_2O_2.(Table 1, entries 8 and 11) The LSV measurements showed that the additives of non-metallic and metallic salts could enhance the electron transfer efficiency of NGO (Figure S11). The cycling/stability tests (Figure S12) and ethanol quenching results (Figure S13) on NGO-A/N were similar to these on NGO-H_2O_2. When the radical pathway was ceased with full ethanol dosage, 34.9% BzH yield was remained compared with 59.1% BzH yield from the no-quenching test, indicating that over half of the performed

341 oxidation was originated from the non-radical reaction. These results provided a convincing proof to

342 the previous conjecture that the N and O were co-active sites in PMS activation for BzOH oxidation.

343 Besides, the oxidation reaction performed under various conditions by adopting NGO-A/N as the

344 representative catalyst showed that the increased temperature, reaction time, catalyst and PMS dosage

345 could lead to improved BzOH conversion and BzH yield (Table S4). The BzH selectivity remained

346 almost at a similar level regardless of the alternation of reaction conditions, indicating that such a

347 highly selective reaction system was quite robust and tolerant for a wide range of working conditions.

348 In this work, the highest BzH yield of 82% was obtained at a PMS/BzOH ratio of 2.5 with 96% BzOH

349 conversion and 85.4% selectivity (Table 1, entry 12), which was the most effective in BzOH oxidation

350 compared with various reaction systems in the reported work but the reaction temperature here was

351 much lower (Table S5). Specifically, this performance was even superior to that of noble-metal (Pd/Pb)

352 catalyst with higher conversion (96 versus 91.3%) and lower temperature (50 versus 130 ºC).

353 **Theoretical calculations to simulate the adsorption behaviour.**

354   **Table 2** The adsorption energy (E_{ads}) of BzOH on graphene and bond length of BzOH molecules in

355 the carbon configurations shown in Figure S14.

Structure	E_{ads} (eV)	l_{C-O} (Å)	l_{O-H} (Å)	l_{C-H}^a (Å)	l_{C-H}^b (Å)
Free BzOH	-	1.432	0.972	1.106	1.106
BzOH@graphene	-0.71	1.431	0.975	1.106	1.102
BzOH@N-graphene	-0.81	1.431	0.977	1.106	1.102
BzOH@C=O-graphene	-0.69	1.432	0.972	1.105	1.107

356   [a] The bond length of αC-H bond was closer to the graphene plane.
357   [b] The bond length of the other αC-H bond of BzOH.
358

359   Adsorption was the prerequisite step in promoting the interactions between the reactant molecules

360 and the doped graphene catalysts. Thus, theoretical calculations were conducted to investigate the

361 adsorption behaviour of BzOH and PMS molecules on various graphene substrates. The relaxed

17

362 structures of the adsorbed BzOH on three carbon models, pure graphene (a), pyridinic N-doped

363 graphene (b), and carbonylated graphene (c), were displayed in Figure S14. The adsorption energy

364 (E_{ads}) and bond length of BzOH molecules obtained from density functional theory (DFT) calculations

365 were summarized in Table 2. The E_{ads} of the three configurations followed the sequence of (b) > (a) >

366 (c), which was in accordance with the effect of electron affinity mentioned above, implying that the

367 BzOH molecules tend to be adsorbed on electrophilic domains. When BzOH was adsorbed on N-

368 graphene (b), the O-H bond was stretched whereas such a stretching phenomenon was not observed

369 on other bonds. Conventional metal-based catalysis suggests that the oxidation of BzOH was initiated

370 by the cleavage of O-H bond.[42-45] It could be inferred that the pyridinic N-doped graphene facilitated

371 the adsorption of BzOH molecules on the electrophilic domains of the carbon and that the stretched

372 O-H bond could be further cleaved to donate an electron to the graphene skeleton.

373   The adsorption of PMS on the edge sites of the three functionalized graphene models and the

374 calculation results were presented in Figure S15 and Table S6. High adsorption energies of PMS were

375 observed on pyridinic N graphene (-3.91 eV) and O=C-graphene (-3.59 eV) as compared with pure

376 graphene (-3.43 eV). Recently, it was found that the electrophilic groups on a carbo-catalyst could

377 activate PMS via the O-H bond cleavage (H-OOSO3) to efficiently generate $SO_5^{\bullet-}$ radicals for

378 subsequent oxidations.[27] Similar calculation results were achieved on PMS/pyridinic N-graphene

379 configuration where the l_{O-H} was remarkably stretched (1.003 versus 0.982 Å of free PMS). The O-O

380 bond of PMS (HO-OSO3) was elongated on O=C-graphene (1.466 versus 1.465 Å in other cases),

381 agreeing with the reported observation that the C=O groups contributed to the breakup of O-O bond

382 of PMS to yield $SO_4^{\bullet-}$ and $^{\bullet}OH$ radicals.[24] Based on the theoretical evidence, it was suggested that

383 both the pyridinic N and carbonyl groups on graphene were responsible for the radical generation by

384 providing electrophilic/nucleophilic domains for PMS adsorption and the O-O/O-H bond cleavage.

385 Besides, the adherent BzOH on pyridinic N and PMS on C=O could create a pair of active sites to

386 enable the non-radical electron transfer pathway.

387　**Mechanism elucidation.**
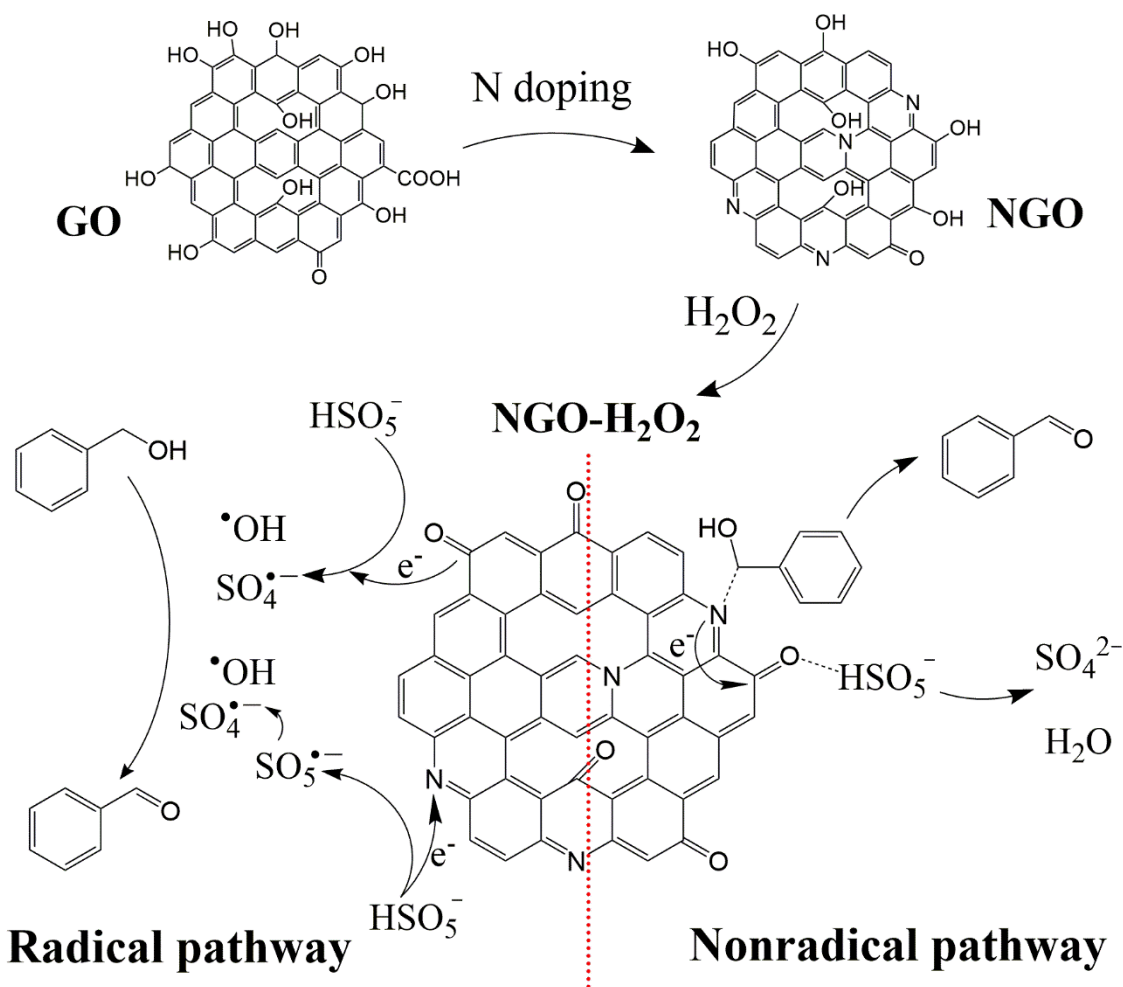
388

389　**Figure 3.** Preparation of the refined N-doped GO and proposed mechanism of the catalytic
390　radical/non-radical pathways for selective oxidation of BzOH.

391　　The proposed mechanism of the reaction pathways using the prepared typical catalyst of NGO-H_2O_2

392　was schematically shown in Figure 3. After N-doping and post-oxidation by H_2O_2, the original GO

393　surface was conferred with abundant pyridinic N and carbonyl species. The NGO-H_2O_2 could activate

394　PMS for selective oxidation of BzOH into BzH via both radical and non-radical processes. When the

395　pyridinic N and C=O species were located closely on the edges of graphene planes, the pyridinic N

396　could induce electrophilic domains on adjacent graphene layers and attract the electron-saturated

397　branch in BzOH whereas the electron-rich C=O groups were related to the -O-O- configuration in

398　PMS. The electron transfer from BzOH to PMS occured subsequently through the highly conjugated

19

399   π system of graphene to accomplish the non-radical pathway with high selectivity. The isolated N and

400   C=O could also adsorb and activate PMS by capturing electrons from PMS to generate $SO_5^{\bullet-}$ radicals

401   (which could be further decomposed into $SO_4^{\bullet-}$ radicals) or donate an electron to PMS to form $SO_4^{\bullet-}$

402   and $^{\bullet}OH$ radicals. The generated reactive radicals would further react with BzOH to generate BzH.

403   The catalyst maintained the electron balance and stability via the transfer of delocalized electrons of

404   graphene for both radical and non-radical processes.

405   **Explanations for highly selective BzOH to BzH without deep-oxidation.**
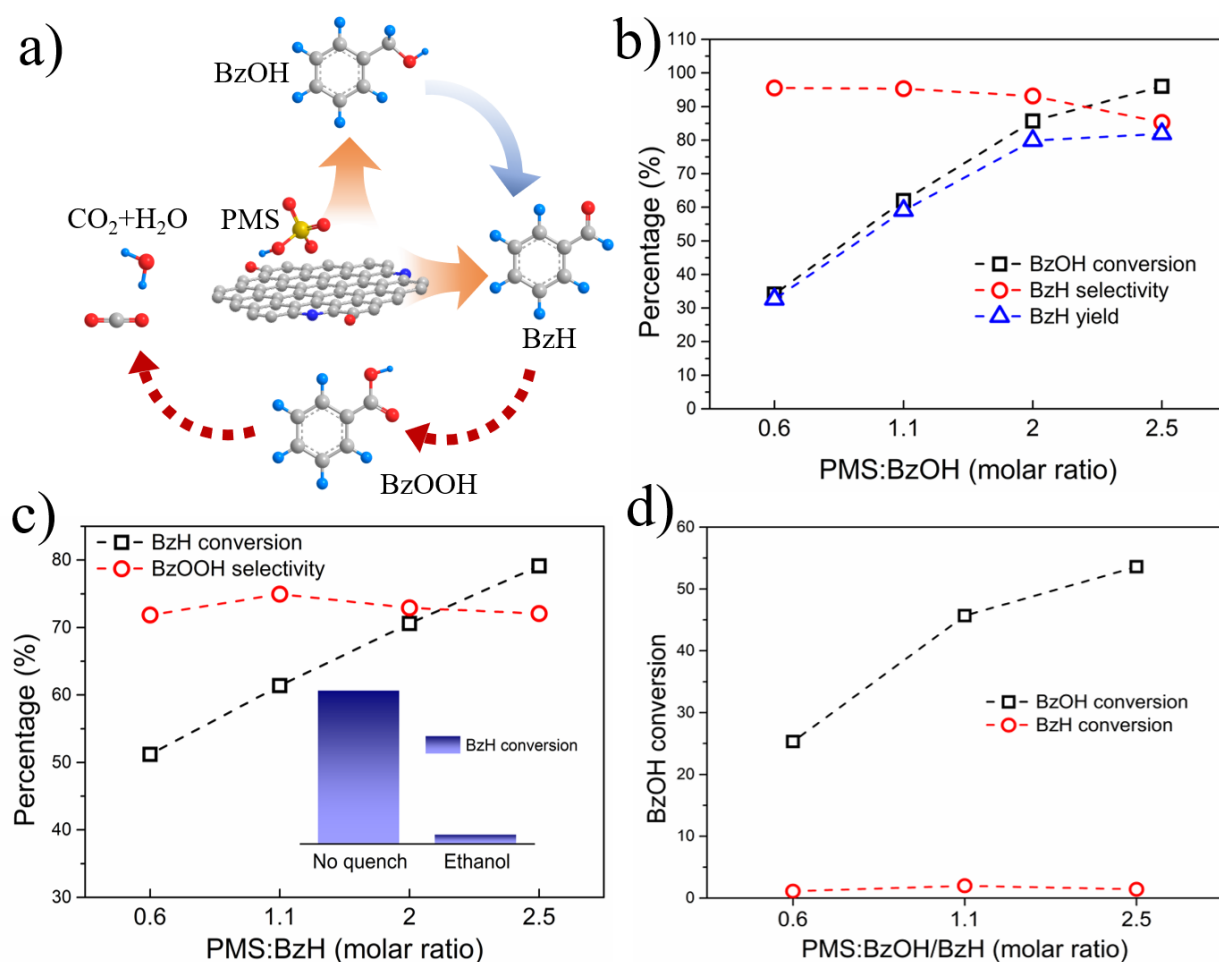
406

407   **Figure 4.** a) The oxidation behaviour of BzOH in PMS/graphene system. b) Oxidation of only

408   BzOH with different PMS dosage. c) Oxidation of only BzH with different PMS dosage (the inset

409   showed the decrease of BzH conversion when the acetonitrile in the solvent was replaced with

410   ethanol). d) Oxidation with the co-existence of BzOH and BzH. Reaction conditions: 5 mg NGO-A/N,

411   0.1 mmol BzOH (applicable to (b) and (d)), 0.1 mmol BzH (applicable to (c) and (d)), 5 mL

412   acetonitrile/water (1:1, volume ratio), 50 ℃, 3 h.

413   In theory, multiple oxidation reactions, as displayed in Figure 4a, could occur during the oxidation

414   of BzOH with the PMS/NGO system. However, the deep-oxidation behaviour from BzH to BzOOH

415   or CO_2 (marked by the red arrows) was not observed. To fully understand the oxidation behaviour,

416   especially BzH free from the deep-oxidation into BzOOH or other products, the individual and

417   competitive reactions of BzOH and BzH towards the PMS/NGO system were performed. Firstly,

418   BzOH and BzH were individually loaded into the reaction system with different PMS dosage. In the

419   case of BzOH solely, its conversion was remarkably increased with higher PMS dosage (Figure 4b).

420   Even at the 2.5-fold PMS dosage, no BzOOH was found in the product, and this suggsted that the

421   higher PMS loading could not lead to the over oxidation of BzH into BzOOH in the presence of BzOH.

422   However, when BzH was served as the oxidation substrate, the result was completely different. BzH

423   was selectively oxidized into BzOOH with 70-80% selectivity free from other organic by-products

424   (Figure 4c). A linear relationship was also observed between the BzH conversion and the added PMS

425   content. Ehanol quenching tests were performed to prove the BzH oxidation pathway, and the result

426   was shownin the inset of Figure 4c. The BzH conversion was sharply reduced to only 3.5% after

427   adding ethanol, compared with 61.4% conversion without quenching. Therefore, the BzH to BzOOH

428   reaction route in the PMS/NGO system was only applicable via radical processes in the absence of

429   BzH. When an identical amount of BzOH and BzH co-existed in the system, the ascending curve of

430   BzOH conversion with the increased PMS dosage was also observed (Figure 4d), much similar to

431   Figure 4b. Under various PMS dosage, the conversion of the initial added BzH was kept below 2%,

432   as calculated according to the selectivity level of Figure 4b, indicating that the original BzH was

433   hardly oxidized because of the co-existed BzOH (Figure 4d and Figure S16). Therefore, it was

suggested that BzH is free from deep-oxidation during the selective oxidation of BzOH due to the unreacted BzOH serving as the shield.

DFT calculations of the adsorption behaviour of BzH on the three different graphene configurations as above, namely plain graphene, N-graphene and C=O-graphene, was also simulated to explain the inhibited deep-oxidation of BzH (Figure S17). The adsorption energies of BzOH and BzH on the same configurations were compared in Table S7. The E_{ads} of BzOH on different graphene templates varied from -0.689 to -0.809 eV, whereas they were only -0.025 eV for BzH adsorption on all three carbon templates. Hence, the BzH molecules were unlikely to be adsorbed on the graphene surface. As a result, the BzH oxidation via the surface-adsorbed non-radical pathway was unlikely to occur. This explained the preliminary result that the BzH could only be oxidized via the radical process in Figure 4c. Moreover, this observation provided convincing evidence that the non-radical oxidation of BzOH was attributed to the electron-transfer via the surface-adsorbed chemicals instead of the widely reported singlet oxygen ($^1O_2$). The $^1O_2$ was proven to be generated via the interaction of catalyst and PMS, regardless of the organic reactant,[46] thus the fact that BzH could only be oxidized by the radicals ruled out the possibility of the oxidation of BzOH by $^1O_2$ since BzH possessed a more oxidizable nature than BzOH.

It has been reported that the α–H from the BzOH molecule could quench the radicals and minimize the autoxidation of BzH,[28] which might help explain the inhibitive effect of BzOH on the radical-based BzH oxidation. To prove that, an identical amount of 1-phenylethanol, toluene and ethylbenzene were added to the BzH oxidation system individually to demonstrate the influence of the α–H-containing benzylic alcohol on BzH oxidation. The results demonstrated that all the added chemicals could inhibit the BzH oxidation, but the inhibition influence was associated with the chemical structures. The 1-phenylethanol molecule with one α–H was less effective in suppressing the BzH conversion compared with BzOH with two α–Hs (Figure S18 and Figure 4d), but still more inhibitive than toluene and ethylbenzene containing no hydroxyl α–H. Based on these observations, it was

459　suggested that the benzylic alcohols with α–H was more reactive than aliphatic C-H towards the

460　radicals and could essentially quench the oxidation of BzH. Overall, the selectivity of the BzOH to

461　BzH in PMS/NGO reaction system could naturally reach a high level and the over oxidation of BzH

462　was favourably blocked via both radical and non-radical routes.

463　　In summary, we report the development of a carbonylated N-doped graphene catalyst for the

464　selective conversion of BzOH into BzH by PMS with high efficiency under benign conditions. Over

465　95% BzOH conversion and 80% BzH yield were achieved on this carbocatalyst via both radical and

466　non-radical processes. The experimental results and DFT calculations were in good agreement to

467　elucidate the radical/non-radical pathways. The doped N species and carbonyl groups (C=O) were

468　found significantly contribute to the enhanced radical and non-radical activities, of which the non-

469　radical oxidation could afford higher BzH selectivity. The integrated dual active sites formed with

470　electron-withdrawing pyridinic N and electron-rich C=O groups could adsorb PMS and BzOH onto

471　the N-doped graphene and build an electron bridge facilitating the electron transfer for the oxidation.

472　Reaction results using the graphene with isolated active sites verified that each of these two functional

473　groups could activate PMS to generate various radicals for subsequent BzOH oxidation. BzH

474　remained to be the sole product under the testing conditions as the deep-oxidation of BzH was

475　inhibited not only in the radical but also in the non-radical route. In light of theoretical calculation,

476　the BzH molecules could hardly be adsorbed on graphene catalysts, disabling its non-radical

477　oxidation. In total the sole BzH as the reactant could be oxidized into BzOOH by the reactive radicals

478　generated from PMS, whereas the presence of BzOH would inhibit this process due to its priority to

479　react with these free radicals. This study revealed the intrinsic nature of the selective reaction via

480　PMS/NGO system for BzOH conversion to BzH, which might provide a versatile strategy using such

481　functionalized graphene catalysts for the selective oxidation of other organics.

482

483 **ASSOCIATED CONTENT**

484 **Supporting Information**.

485 Supplementary material, characterizations and catalytic results (Tables S1-S7 and Figures S1-S18)

486 **AUTHOR INFORMATION**

487 **Corresponding Authors**

488 *S.B. Wang. shaobin.wang@curtin.edu.au

489 *J.W. Tang. Junwang.tang@ucl.ac.uk

490 *S.M. Liu. shaomin.liu@curtin.edu.au

491 **Author Contributions**

492 J.L. performed all the experiments, data analysis and drafted this article. Q.Y. and Q.N.Y.

493 contributed to the review and polishing. S.W., H.S., J.T., X.Z. and S.L. contributed to the mechanistic

494 proposal of this work and the revision of this manuscript.

495

496 ABBREVIATIONS

497 BzOH, benzyl alcohol; BzH, benzaldehyde; TBHP, *tert*-butyl hydroperoxide; PMS,

498 peroxymonosulfate; AOPs, advanced oxidation processes; BzOOH, benzoic acid; NGO, nitrogen-

499 doped graphene oxides; MWCNT, multi-walled carbon nanotubes; SWCNT, single-walled carbon

500 nanotubes; AC, active carbon; ND, nanodiamond; TBA, *tert*-butanol; PH, phenylhydrazine.

501

502 **Notes**

503 The authors declare no competing financial interests.

References

1.   Luo, J.; Yu, H.; Wang, H.; Wang, H.; Peng, F., Aerobic oxidation of benzyl alcohol to benzaldehyde catalyzed by carbon nanotubes without any promoter. *Chemical Engineering Journal* **2014,** *240*, 434-442.

2.   Choudhary, V. R.; Dhar, A.; Jana, P.; Jha, R.; Uphade, B. S., A green process for chlorine-free benzaldehyde from the solvent-free oxidation of benzyl alcohol with molecular oxygen over a supported nano-size gold catalyst. *Green Chemistry* **2005,** *7* (11), 768-770.

3.   Wang, H.; Wang, C.; Yan, H.; Yi, H.; Lu, J., Precisely-controlled synthesis of Au@Pd core–shell bimetallic catalyst via atomic layer deposition for selective oxidation of benzyl alcohol. *Journal of Catalysis* **2015,** *324*, 59-68.

4.   Makwana, V. D.; Son, Y.-C.; Howell, A. R.; Suib, S. L., The Role of Lattice Oxygen in Selective Benzyl Alcohol Oxidation Using OMS-2 Catalyst: A Kinetic and Isotope-Labeling Study. *Journal of Catalysis* **2002,** *210* (1), 46-52.

5.   Parmeggiani, C.; Matassini, C.; Cardona, F., A step forward towards sustainable aerobic alcohol oxidation: new and revised catalysts based on transition metals on solid supports. *Green Chemistry* **2017,** *19* (9), 2030-2050.

6.   Long, J.; Xie, X.; Xu, J.; Gu, Q.; Chen, L.; Wang, X., Nitrogen-Doped Graphene Nanosheets as Metal-Free Catalysts for Aerobic Selective Oxidation of Benzylic Alcohols. *ACS Catalysis* **2012,** *2* (4), 622-631.

7.   Yongbo, K.; M., I. N.; Yuta, N.; Teruaki, H.; Masa‐aki, K., Selective Aerobic Oxidation of Benzylic Alcohols Catalyzed by Carbon‐Based Catalysts: A Nonmetallic Oxidation System. *Angewandte Chemie International Edition* **2010,** *49* (2), 436-440.

8.   R., D. D.; Hong‐Peng, J.; W., B. C., Graphene Oxide: A Convenient Carbocatalyst for Facilitating Oxidation and Hydration Reactions. *Angewandte Chemie* **2010,** *122* (38), 6965-6968.

9.   Sheng, S. D.; Guodong, W.; Shuchang, W.; Feng, P.; Robert, S., Carbocatalysis in Liquid‐Phase Reactions. *Angewandte Chemie International Edition* **2017,** *56* (4), 936-964.

10.   Hussain, H.; Green, I. R.; Ahmed, I., Journey Describing Applications of Oxone in Synthetic Chemistry. *Chemical Reviews* **2013,** *113* (5), 3329-3371.

11.   Neyens, E.; Baeyens, J., A review of classic Fenton's peroxidation as an advanced oxidation technique. *Journal of Hazardous Materials* **2003,** *98* (1), 33-50.

12.   Choudhary, V. R.; Dumbre, D. K., Solvent-free selective oxidation of benzyl alcohol to benzaldehyde by tert-butyl hydroperoxide over U3O8-supported nano-gold catalysts. *Applied Catalysis A: General* **2010,** *375* (2), 252-257.

13.   Hu, P.; Long, M., Cobalt-catalyzed sulfate radical-based advanced oxidation: A review on heterogeneous catalysts and applications. *Applied Catalysis B: Environmental* **2016,** *181*, 103-117.

14.   Mello, R.; Cassidei, L.; Fiorentino, M.; Fusco, C.; Hummer, W.; Jager, V.; Curci, R., OXIDATIONS BY METHYL(TRIFLUOROMETHYL)DIOXIRANE .5. CONVERSION OF ALCOHOLS INTO CARBONYL-COMPOUNDS. *Journal of the American Chemical Society* **1991,** *113* (6), 2205-2208.

546   15.   Thottumkara, A. P.; Bowsher, M. S.; Vinod, T. K., In Situ Generation of o-Iodoxybenzoic
547   Acid (IBX) and the Catalytic Use of It in Oxidation Reactions in the Presence of Oxone as a Co-
548   oxidant. *Organic Letters* **2005,** *7* (14), 2933-2936.
549   16.   Schulze, A.; Giannis, A., Oxidation of Alcohols with Catalytic Amounts of IBX. *Synthesis*
550   **2006,** *2006* (02), 257-260.
551   17.   Page, P. C. B.; Appleby, L. F.; Buckley, B. R.; Allin, S. M.; McKenzie, M. J., In Situ
552   Generation of 2-Iodoxybenzoic Acid (IBX) in the Presence of Tetraphenylphosphonium
553   Monoperoxysulfate (TPPP) for the Conversion of Primary Alcohols into the Corresponding
554   Aldehydes. *Synlett* **2007,** *2007* (10), 1565-1568.
555   18.   Uyanik, M.; Ishihara, K., Hypervalent iodine-mediated oxidation of alcohols. *Chemical*
556   *Communications* **2009,** (16), 2086-2099.
557   19.   Uyanik, M.; Akakura, M.; Ishihara, K., 2-Iodoxybenzenesulfonic Acid as an Extremely
558   Active Catalyst for the Selective Oxidation of Alcohols to Aldehydes, Ketones, Carboxylic Acids,
559   and Enones with Oxone. *Journal of the American Chemical Society* **2009,** *131* (1), 251-262.
560   20.   Koo, B.-S.; Lee, C. K.; Lee, K.-J., OXIDATION OF BENZYL ALCOHOLS WITH
561   OXONE® AND SODIUM BROMIDE. *Synthetic Communications* **2002,** *32* (14), 2115-2123.
562   21.   Duan, X.; Sun, H.; Kang, J.; Wang, Y.; Indrawirawan, S.; Wang, S., Insights into
563   Heterogeneous Catalysis of Persulfate Activation on Dimensional-Structured Nanocarbons. *ACS*
564   *Catalysis* **2015,** *5* (8), 4629-4636.
565   22.   Sun, H.; Liu, S.; Zhou, G.; Ang, H. M.; Tadé, M. O.; Wang, S., Reduced Graphene Oxide for
566   Catalytic Oxidation of Aqueous Organic Pollutants. *ACS Applied Materials & Interfaces* **2012,** *4*
567   (10), 5466-5471.
568   23.   Duan, X.; Ao, Z.; Sun, H.; Indrawirawan, S.; Wang, Y.; Kang, J.; Liang, F.; Zhu, Z. H.;
569   Wang, S., Nitrogen-Doped Graphene for Generation and Evolution of Reactive Radicals by Metal-
570   Free Catalysis. *ACS Applied Materials & Interfaces* **2015,** *7* (7), 4169-4178.
571   24.   Duan, X.; Sun, H.; Ao, Z.; Zhou, L.; Wang, G.; Wang, S., Unveiling the active sites of
572   graphene-catalyzed peroxymonosulfate activation. *Carbon* **2016,** *107*, 371-378.
573   25.   Duan, X.; Ao, Z.; Zhou, L.; Sun, H.; Wang, G.; Wang, S., Occurrence of radical and
574   nonradical pathways from carbocatalysts for aqueous and nonaqueous catalytic oxidation. *Applied*
575   *Catalysis B: Environmental* **2016,** *188*, 98-105.
576   26.   Duan, X.; Sun, H.; Wang, Y.; Kang, J.; Wang, S., N-Doping-Induced Nonradical Reaction
577   on Single-Walled Carbon Nanotubes for Catalytic Phenol Oxidation. *ACS Catalysis* **2015,** *5* (2),
578   553-559.
579   27.   Li, J.; Li, M.; Sun, H.; Ao, Z.; Wang, S.; Liu, S., Understanding of the Oxidation Behavior
580   of Benzyl Alcohol by Peroxymonosulfate via Carbon Nanotubes Activation. *ACS Catalysis* **2020,** *10*
581   (6), 3516-3525.
582   28.   Sankar, M.; Nowicka, E.; Carter, E.; Murphy, D. M.; Knight, D. W.; Bethell, D.; Hutchings,
583   G. J., The benzaldehyde oxidation paradox explained by the interception of peroxy radical by benzyl
584   alcohol. *Nature Communications* **2014,** *5* (1), 3332.
585   29.   Li, D.; Duan, X.; Sun, H.; Kang, J.; Zhang, H.; Tade, M. O.; Wang, S., Facile synthesis of
586   nitrogen-doped graphene via low-temperature pyrolysis: The effects of precursors and annealing
587   ambience on metal-free catalytic oxidation. *Carbon* **2017,** *115*, 649-658.
588   30.   Arrigo, R.; Hävecker, M.; Wrabetz, S.; Blume, R.; Lerch, M.; McGregor, J.; Parrott, E. P. J.;
589   Zeitler, J. A.; Gladden, L. F.; Knop-Gericke, A.; Schlögl, R.; Su, D. S., Tuning the Acid/Base
590   Properties of Nanocarbons by Functionalization via Amination. *Journal of the American Chemical*
591   *Society* **2010,** *132* (28), 9616-9630.
592   31.   Kundu, S.; Xia, W.; Busser, W.; Becker, M.; Schmidt, D. A.; Havenith, M.; Muhler, M., The
593   formation of nitrogen-containing functional groups on carbon nanotube surfaces: a quantitative XPS
594   and TPD study. *Physical Chemistry Chemical Physics* **2010,** *12* (17), 4351-4359.

595   32.   Chen, Z.; Higgins, D.; Chen, Z., Nitrogen doped carbon nanotubes and their impact on the
596   oxygen reduction reaction in fuel cells. *Carbon* **2010,** *48* (11), 3057-3065.
597   33.   Yang, H. B.; Miao, J.; Hung, S.-F.; Chen, J.; Tao, H. B.; Wang, X.; Zhang, L.; Chen, R.;
598   Gao, J.; Chen, H. M.; Dai, L.; Liu, B., Identification of catalytic sites for oxygen reduction and
599   oxygen evolution in N-doped graphene materials: Development of highly efficient metal-free
600   bifunctional electrocatalyst. *Science Advances* **2016,** *2* (4), e1501122.
601   34.   Zhang, J.; Liu, X.; Blume, R.; Zhang, A.; Schlögl, R.; Su, D. S., Surface-Modified Carbon
602   Nanotubes Catalyze Oxidative Dehydrogenation of *n*-Butane. *Science* **2008,** *322* (5898), 73.
603   35.   Li, J.; Yu, P.; Xie, J.; Liu, J.; Wang, Z.; Wu, C.; Rong, J.; Liu, H.; Su, D., Improving the
604   Alkene Selectivity of Nanocarbon-Catalyzed Oxidative Dehydrogenation of n-Butane by
605   Refinement of Oxygen Species. *ACS Catalysis* **2017,** *7* (10), 7305-7311.
606   36.   Tuinstra, F.; Koenig, J. L., Raman Spectrum of Graphite. *The Journal of Chemical Physics*
607   **1970,** *53* (3), 1126-1130.
608   37.   Chua, C. K.; Pumera, M., Renewal of sp2 bonds in graphene oxides via dehydrobromination.
609   *Journal of Materials Chemistry* **2012,** *22* (43), 23227-23231.
610   38.   Qin, L.; Wang, L.; Wang, C.; Yang, X.; Lv, B., Enhanced role of graphitic-N on nitrogen-
611   doped porous carbon ball for direct dehydrogenation of ethylbenzene. *Molecular Catalysis* **2019,**
612   *462*, 61-68.
613   39.   Qi, W.; Liu, W.; Zhang, B.; Gu, X.; Guo, X.; Su, D., Oxidative Dehydrogenation on
614   Nanocarbon: Identification and Quantification of Active Sites by Chemical Titration. *Angewandte*
615   *Chemie International Edition* **2013,** *52* (52), 14224-14228.
616   40.   Zhang, Y.; Wang, J.; Rong, J.; Diao, J.; Zhang, J.; Shi, C.; Liu, H.; Su, D., A Facile and
617   Efficient Method to Fabricate Highly Selective Nanocarbon Catalysts for Oxidative
618   Dehydrogenation. *ChemSusChem* **2017,** *10* (2), 353-358.
619   41.   Diao, J.; Zhang, Y.; Zhang, J.; Wang, J.; Liu, H.; Su, D. S., Fabrication of MgO–rGO hybrid
620   catalysts with a sandwich structure for enhanced ethylbenzene dehydrogenation performance.
621   *Chemical Communications* **2017,** *53* (82), 11322-11325.
622   42.   Yamaguchi, K.; Mizuno, N., Supported Ruthenium Catalyst for the Heterogeneous
623   Oxidation of Alcohols with Molecular Oxygen. *Angewandte Chemie International Edition* **2002,** *41*
624   (23), 4538-4542.
625   43.   Aellig, C.; Girard, C.; Hermans, I., Aerobic Alcohol Oxidations Mediated by Nitric Acid.
626   *Angewandte Chemie International Edition* **2011,** *50* (51), 12355-12360.
627   44.   Zhou, C.; Chen, Y.; Guo, Z.; Wang, X.; Yang, Y., Promoted aerobic oxidation of benzyl
628   alcohol on CNT supported platinum by iron oxide. *Chemical Communications* **2011,** *47* (26), 7473-
629   7475.
630   45.   Ng, Y. H.; Ikeda, S.; Morita, Y.; Harada, T.; Ikeue, K.; Matsumura, M., Origin of the High
631   Activity of Porous Carbon-Coated Platinum Nanoparticles for Aerobic Oxidation of Alcohols. *The*
632   *Journal of Physical Chemistry C* **2009,** *113* (29), 12799-12805.
633   46.   Jawad, A.; Zhan, K.; Wang, H.; Shahzad, A.; Zeng, Z.; Wang, J.; Zhou, X.; Ullah, H.; Chen,
634   Z.; Chen, Z., Tuning of Persulfate Activation from a Free Radical to a Nonradical Pathway through
635   the Incorporation of Non-Redox Magnesium Oxide. *Environmental Science & Technology* **2020,** *54*
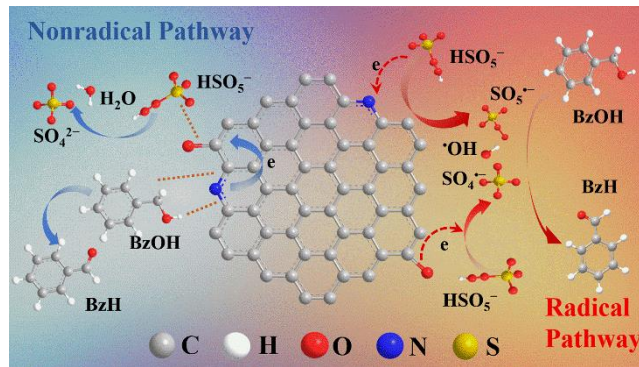636   (4), 2476-2488.

637

638

639

640

641   **Table of Contents**

642

643